Magnetocaloric effect and evidence of superparamagnetism in $GdAl_2$ nanocrystallites: A magnetic-structural correlation

V. G. de Paula,[1] L. M. da Silva,[2,*] A. O. dos Santos,[2] R. Lang,[3] L. Otubo,[4] A. A. Coelho,[1] and L. P. Cardoso[1]

[1]*Instituto de Física Gleb Wataghin, Universidade Estadual de Campinas-UNICAMP, 13083-859 Campinas, São Paulo, Brazil*

[2]*Centro de Ciências Sociais, Saúde e Tecnologia (CCSST), Universidade Federal do Maranhão-UFMA, 65900-000 Imperatriz, Maranhão, Brazil*

[3]*Instituto de Ciência e Tecnologia-ICT, UNIFESP, 12231-280 São José dos Campos, São Paulo, Brazil*

[4]*Centro de Ciência e Tecnologia de Materiais, Instituto de Pesquisas Energéticas e Nucleares-IPEN, 05508-000 São Paulo, São Paulo, Brazil*

(Received 22 December 2015; revised manuscript received 23 February 2016; published 23 March 2016)

The correlation between structural and magnetic properties of $GdAl_2$, focusing on the role played by the disorder in magnetic ordering and how it influences the magnetocaloric effect (MCE) are discussed. Micrometric-sized particles, consisting of nanocrystallites embedded in an amorphous matrix, were prepared by a mechanical milling technique and characterized by means of x-ray diffraction, scanning and high-resolution transmission electron microscopy as well as magnetic measurements as a function of an applied external magnetic field and temperature. The results show that the average particle size is just slightly diminished ($\approx$7%) with the milling time (between 3 and 13 h), whereas the average crystallite size undergoes an expressive reduction ($\approx$43%). For long milling times, structural disorders mostly associated with crystallite size singularly affect the magnetic properties, leading to a large tablelike MCE in the temperature range between 30 and 165 K. Below 30 K, nanocrystallites with dimensions below a given critical size cause an enhancement in the magnetic entropy change related to superparamagnetic behavior. In contrast, for low milling times, relative cooling power values are improved. These striking features along with the small magnetic hysteresis observed make the milled $GdAl_2$ a promising material for application in the magnetic refrigeration technology. Finally, a discussion in an attempt to elucidate the origin of the spin-glass states previously reported in the literature for mechanically milled $GdAl_2$ samples for very long times (400 and 1000 h) is presented.

DOI: 10.1103/PhysRevB.93.094427

I. INTRODUCTION

The magnetocaloric effect (MCE), which is characterized as the heating or the cooling of material under an applied magnetic-field change, has been the object of extensive studies aiming at practical applications, such as in magnetic refrigeration devices. It is an environment-friendly and a more efficient refrigeration technique when compared to the conventional refrigeration technology—traditional gas compression and/or expansion [1–3]. One of the challenges in materials science and engineering is to find magnetic materials with suitable characteristics (such as a high effective magnetic moment and the existence of magnetic/structural transitions) to produce a large MCE under low applied magnetic field (permanent magnets range) without thermal and magnetic hysteresis losses [4,5]. In addition, it is desirable to obtain the maximum effect occurring in a large range of temperatures (tablelike behavior) [6].

Most of the studies have been directed at bulk magnetic materials for different families of compounds that present first- or second-order magnetic transition [7–17]. However, it is well known that magnetic properties are strongly dependent on the structure and material size; and nanostructured magnetocaloric materials in the form of thin films and nanoalloys have attracted a noticeable interest and stimulated intense experimental activity in this field [18–21]. Nanoalloys (bi- or multicomponent metallic materials) can be produced by different synthesis methods and assume several morphologies, which can originate a large diversity of physical and chemical properties [22–25]. Some reports on nanoalloys based on rare-earth (R) intermetallic compounds as RCo_2 (R = Dy and Ho) and RAl_2 (R = Ho and Tb), where R atoms have large magnetic moments, have presented considerable MCE values (between 13 and 25 J kg^{-1} K^{-1} at 50 kOe) at low temperatures due to the nanoscale magnetic properties [26–29]. However, to our knowledge, little attention has been spent on intermediate range, i.e., alloys on the micrometric scale.

Since the magnetic behavior of the micro- and nanosized structures differs from the correspondent bulk ones, exploring magnetic materials within these size ranges is of fundamental importance and can reveal novel promising materials and complement low-dimensional structures knowledge for refrigeration applications.

Here, a milled $GdAl_2$ intermetallic compound is presented for such investigation [30–32]. A previous study shows that crystalline $GdAl_2$ has ferromagnetic (FM) transition at Curie Temperature T_C = 170 K, a small intrinsic anisotropy, and anomalous magnetoelastic behavior [33–35], whereas amorphous $GdAl_2$ thin films present spin-glass (SG) behavior below 16 K [36,37]. A SG state has also been observed in $GdAl_2$ nanostructures obtained by the mechanical milling technique; a case of samples milled for a very long time: 1000 h [30,31]. Posteriorly, the role of the disorder in $GdAl_2$ samples milled for 400 h was discussed, and a model in an attempt to explain the SG effect was proposed [32]. However, the authors conclude that to understand the mechanism of glassy transition in this system it would be necessary to determine the process by which the glassy system was achieved.

Recently, it has been demonstrated that $GdAl_2$-based compounds have a significant magnetocaloric effect due to

*Corresponding author: luzeli.moreira@ufma.br

second-order ferromagnetic phase transition [38–40]. Moreover, studies on $GdAl_2/Al_2O_3$ in the form of nanocapsules have shown a large magnetic entropy change (18.7 $J\,kg^{-1}\,K^{-1}$ at 60 kOe) at low temperatures, which was argued as superparamagnetic contribution [41].

Considering the dissimilar but notable properties observed for $GdAl_2$ in different morphologies (bulk, films, nanocapsules, and nanoparticles), a comprehensive study on the magnetocaloric and material properties of microparticles is of interest and can help a clear an understanding on how such properties and their correlations evolve from bulk to nanoscale.

The present paper reports the material synthesis and a thorough characterization (structural, morphological, and magnetic) of $GdAl_2$ microparticles obtained by a mechanical milling technique in a lower milling time (up to 13 h). Interestingly, the results show that the microparticles are formed by an amorphous matrix with embedded nanocrystallites. High-resolution transmission electron microscopy was employed as a tool to provide a consistent picture of the correlation between structural and magnetic properties. The role played by the disorder in magnetic ordering and how it influences the magnetocaloric effect are discussed.

II. EXPERIMENT

The starting alloys were prepared by arc melting of high-purity elements (Gd = 99.9% and Al = 99.9999%) in an Ar_2 atmosphere. Arc melting was repeated for four times in order to obtain a homogeneous sample. The melted sample was submitted to a thermal annealing at 800 °C for 5 days. The resulting alloy (≈5 g) was crushed and milled in a planetary ball mill (Fritsch Pulverisette 7) at a rotation speed of 200 rpm using a hardened steel container under Ar_2 atmosphere. The milling was carried out in a sequence of 30 min milling and 10 min resting. After every 2 h the container was opened to uncompress the powder. Small amounts of material were collected after 3, 5, 9, and 13 h of milling for the undertaking of studies; always keeping the ball-sample weight ratio about 12. The collected samples were stored under argon atmosphere to avoid oxidation.

Powder x-ray diffraction (XRD) measurements were performed at room temperature by using a Rigaku Miniflex II diffractometer with Cu $K\alpha_1$(1.5406 Å) radiation. The diffraction patterns were obtained in the range of 2θ between 20° and 85° with steps of 0.02° and an acquisition time of 2 s. The crystalline phase was identified through the Rietveld refinement using the GSAS program [42]. The morphology and structure of the powders were analyzed and characterized by scanning electron microscopy (SEM) observations (Philips XL30 electron microscopy—operated at an accelerating voltage of 20 kV) and by high-resolution transmission electron microscopy (HRTEM) images (JEOL JEM-2100 operating at 200 kV) with an energy-dispersive x-ray spectroscopy analyzer (EDX) integrated. SEM samples were prepared by directly spreading the powder over a carbon tape and coated with Au by sputtering. TEM samples were prepared by dropping isopropanol sample suspensions on a 400 mesh copper grid coated with a collodion film. A SQUID (superconducting quantum interference device) magnetometer and a PPMS (Physical Properties Measurement System), both from Quantum Design, Inc., were employed to measure the magnetization (in the temperature interval between 2 and 300 K under applied magnetic fields up to 50 kOe) and the magnetic susceptibility (in the frequency range of 0.05 up to 2 kHz), respectively. To perform the magnetic measurements, small amounts (≈40 mg) of material after the milling process were collected, put into gelatin capsules, and fastened with polystyrene to avoid rotation of particles when being magnetized.

III. RESULTS AND DISCUSSION

Figure 1(a) shows the XRD measurements of the $GdAl_2$ unmilled sample (referred to as 0 h bulk) as well as the XRD measurements of the samples submitted to 3, 5, 9, and 13 h of milling. The $GdAl_2$ compound was found to crystallize in the cubic $MgCu_2$ fcc structure, in agreement with previous results [32]. All reflections were identified, and no spurious phase was detected, i.e., no evidence of contamination from the milling materials or oxidation was observed. As the milling time increases the x-ray diffraction patterns show a reduction in peak intensity and a consequent broadening.

XRD Rietveld refinement analysis was carried out for the entire set of samples (bulk and milled). Figure 1(b) depicts in particular the refinement for the sample milled for 13 h as an example. The analyses confirm that all samples crystallize in the cubic $MgCu_2$ structure; and from the results were extracted average crystallite size, lattice parameter, and microstrain

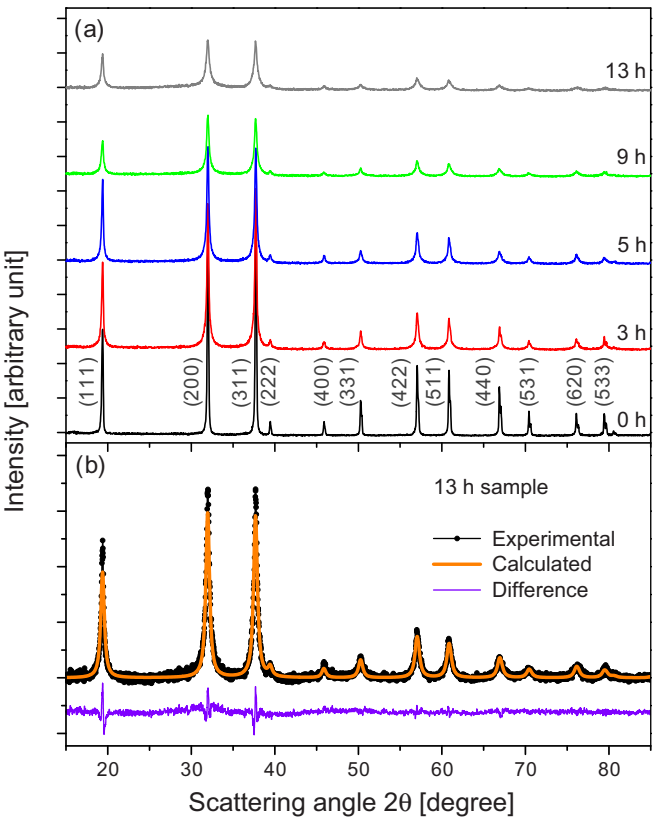

FIG. 1. (a) X-ray-diffraction patterns of the $GdAl_2$ samples: bulk (0 h) and milled for different times: 3, 5, 9, and 13 h. All reflections belong to cubic $MgCu_2$ fcc structure. (b) Best fitting result of the XRD Rietveld refinement for the sample milled for 13 h.

TABLE I. Values of average crystallite size, lattice parameter, and microstrain obtained from XRD Rietveld refinement analyses. The standard deviation is considered between the parentheses.

Milling time (h)	Average crystallite size (nm)	Lattice parameter (Å)	Microstrain (%)
0	90.4(1)	7.8988(6)	0
3	33.2(2)	7.8985(6)	0.03
5	30.9(2)	7.8984(7)	0.09
9	24.1(3)	7.8993(7)	0.13
13	18.8(5)	7.8991(6)	0.14

TABLE II. Values of average particle size, standard deviation, minimum and maximum sizes, and average diameter of 90% of the particles' population obtained from histograms of the SEM images.

Milling time (h)	Particle numbers analyzed	Average particle size (μm)	Standard deviation (μm)	Min./max. size (μm)	D_{90} (μm)
3	211	1.38	0.59	0.47/5.81	2.09
5	212	1.33	0.45	0.43/4.46	2.03
9	218	1.29	0.74	0.38/3.42	1.92
13	204	1.28	0.69	0.34/3.16	1.82

values. Table I shows the results obtained. The average crystallite size decreases considerably with increasing milling time whereas the lattice parameter remained practically constant. However, the increase in microstrain value with increasing milling time indicates that there was the occurrence of lattice deformation (structural disorder) in the $GdAl_2$ crystallites due to the mechanical milling process.

Figure 2 shows representative SEM images of the $GdAl_2$ powder after milling for (a) 3, (b) 5, (c) 9, and (d) 13 h. As can be noticed, the powders have irregular-shaped microstructures, and there is no evidence of spherical particles. Although visually very similar, the average particle size distribution measured for each sample was shown to be slightly different. Table II shows the quantitative results extracted from histograms' analysis of the SEM images. Because of their irregular-shaped morphology, the particle sizes were manually measured from the SEM images. The histograms were constructed and fitted using the normal density function (Gaussian distribution). The average particle size estimated for the sample milled for 3 h [Fig. 2(a)] is about 1.38 ± 0.59 μm, ranging from 0.47 to 5.81 μm, whereas for the sample milled for 5 h [Fig. 2(b)] is about 1.33 ± 0.45 μm, ranging from 0.43 to 4.46 μm. For the sample milled for 9 h [Fig. 2(c)] the average particle size evaluated is about 1.29 ± 0.74 μm, ranging from 0.38 to 3.42 μm, and for the sample milled for 13 h [Fig. 2(d)] the average particle size is about 1.28 ± 0.69 μm, ranging from 0.34 to 3.16 μm. The particle size distribution is also rather different when comparing the population size distribution; 90% of the particles have an average diameter (D_{90}) smaller than $\approx$2.09 μm after milling for 3 h, smaller than $\approx$2.03 μm after milling for 5 h, smaller than $\approx$1.92 μm after milling for 9 h, and smaller than $\approx$1.82 μm after milling for 13 h. To summarize, the histogram results show a slight tendency of decreasing particle size with increasing milling time.

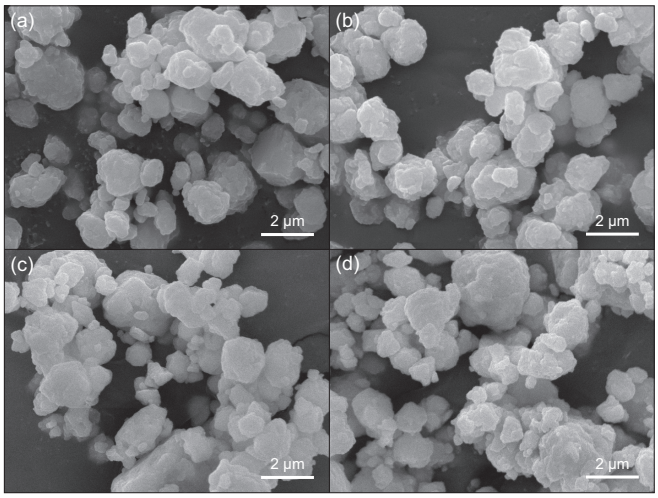

FIG. 2. SEM micrographs of the $GdAl_2$ powder milled for different times: (a) 3, (b) 5, (c) 9, and (d) 13 h.

Qualitative analysis by energy-dispersive x-ray spectroscopy (EDX spectrum and elemental line scan) over a small particle from sample milled for 13 h is shown in Fig. 3. The EDX spectrum [Fig. 3(a)] confirms the presence of the Gd and Al metals that primarily compose the particles besides the Cu. The Cu peaks are originated from the Cu grid used as a sample holder. The line-scan analysis [Fig. 3(b)] shows the profile of composition along the arrow over the particle (the inset). It shows that the particle composition is constant, only varying the intensity of the signals (counts) due to the thickness of the particle.

In seeking a more meaningful distinction, TEM analyses were performed. Figure 4 shows bright-field HRTEM observations of the $GdAl_2$ powders. The images of the samples milled for 3, 5, 9, and 13 h shown as Figs. 4(a)–4(d), respectively, reveal an amorphous matrix with embedded nanocrystallites, at least near the particles' surface region where TEM characterizations were performed. The nanocrystalline grains are randomly oriented in the matrix. Moreover, it is possible to identify an "amorphous shell" produced by mechanical milling. The thickness of this shell is not homogeneous; however, the average thickness increases with the milling time. The insets, Figs. 4(e)–4(h), are fast Fourier transform (FFT) patterns obtained from single grains as pointed out by each selected area. The respective zone axes are depicted in the insets. All FFT patterns correspond to the $GdAl_2$ fcc structure.

Figure 5 presents the average values of the particle (determined by histograms of the SEM images) and of crystallite size (obtained by x-ray data through the Rietveld method) as a function of the milling time. The results indicate reductions of $\approx$43% in the average crystallite size and of $\approx$7% in the average particle size. Furthermore, according to the SEM data the average diameter of 90% of the particles (D_{90}) decreased by $\approx$13%. It is remarkable to notice the decrease in crystallite size as the main effect of the mechanical milling in the used time range (3–13 h).

Figure 6 show results of magnetization as a function of the temperature. The temperature dependences of the

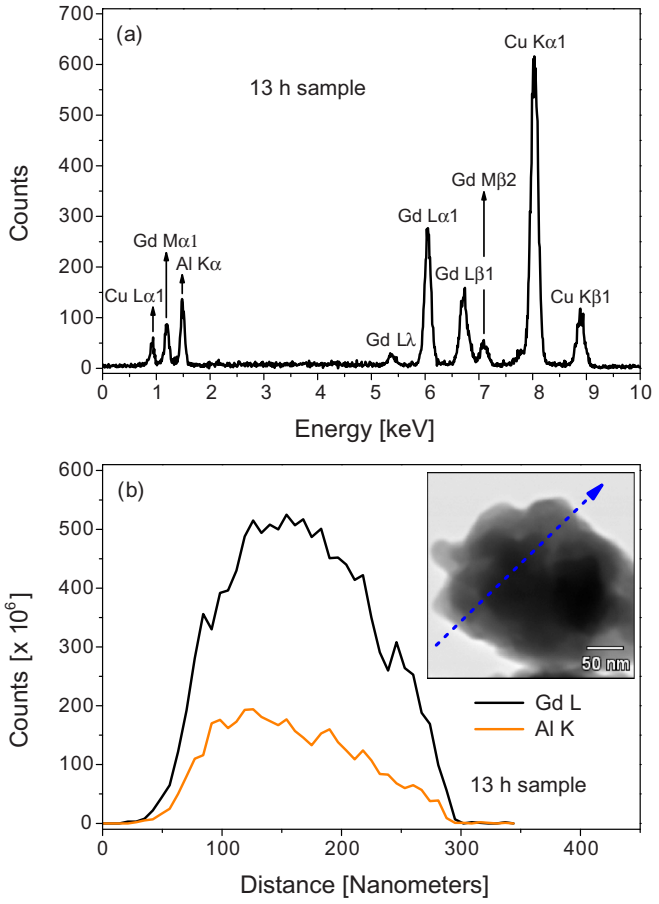

FIG. 3. Energy-dispersive x-ray spectroscopy analysis over a small particle from sample milled for 13 h. (a) EDX spectrum and (b) elemental line scan.

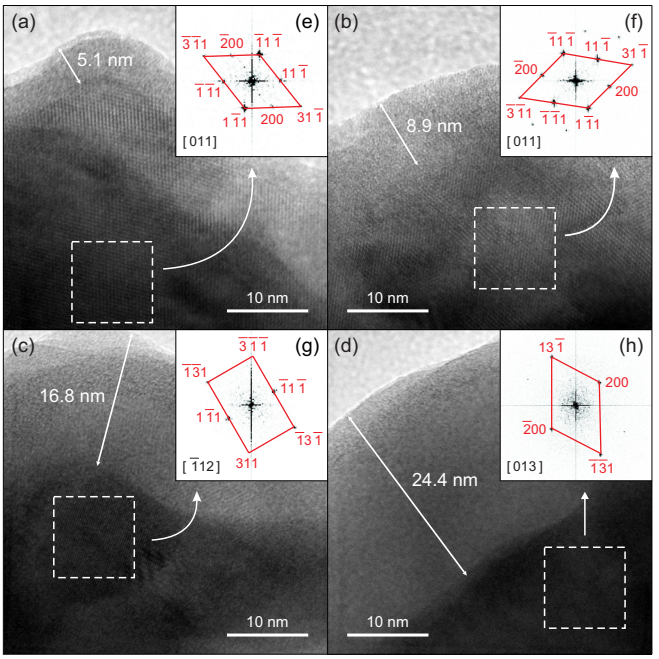

FIG. 4. HRTEM images of the $GdAl_2$ powder milled for different times: (a) 3, (b) 5, (c) 9, and (d) 13 h. The insets (e)–(h) depict fast Fourier transform (FFT) analysis of selected areas in (a)–(d), respectively. All FFT patterns correspond to the $GdAl_2$ fcc structure.

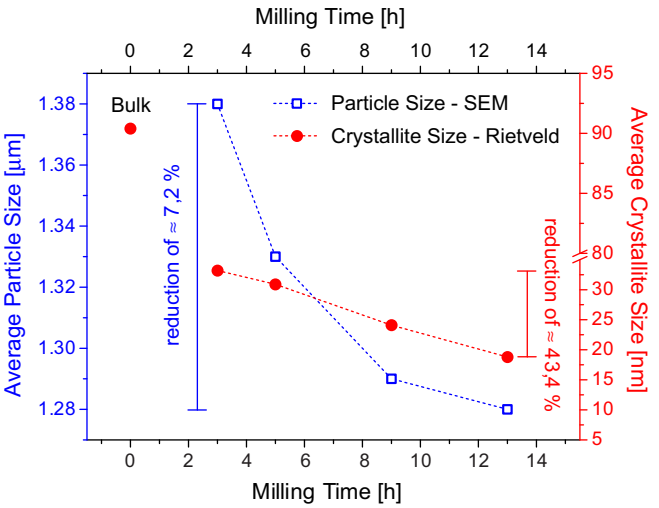

FIG. 5. Average values of particle (left scale) and of crystallite (right scale) size as a function of the milling time for $GdAl_2$ samples.

zero-field-cooling (ZFC) and of the field-cooling (FC) magnetizations for the $GdAl_2$ bulk sample and for the milled samples, under 200 Oe applied magnetic fields, are shown in Fig. 6(a) and in the respective inset. As can be noticed, the FM transition significantly broadens with the increase in the milling time. The T_C obtained for the 0 h sample was about 170 K, which is in good agreement with the values reported for $GdAl_2$ bulk [34]. A small (≈ 2 K) T_C shift to lower temperatures is observed for the 3 h milling sample when compared to the 0 h sample. However, no further shift (greater than ≈ 2 K) could be detected for longer milling times. In fact, it would be expected that T_C shifts with the reduction in the particle size mainly due to the following factors: (i) decreased particle size, interrupting the long-range interaction in the magnetic lattice and (ii) inhomogeneity caused by disorder within the grain [43,44]. Since the average particle size is only slightly decreased with the milling process, it is hard to expect a T_C decrease. In addition, the long-range interaction apparently was not affected by the large crystallite reduction. Hence, the absence of a significant increase in the T_C shift with the milling time increase allows concluding that the small reduction of T_C (≈ 2 K) is associated with structural disorder induced by the milling process. In other words, despite the disorder increases for longer milling times, the T_C shift is more evident for the sample milled for 3 h. A larger shift on T_C for the 5, 9, and 13 h samples could not be inferred due to the inaccuracy in determining the T_C value caused by the FM transition broadening. The broadening of the FM transition with the milling time is, therefore, a result of a T_C distribution, which originates from different degrees of disorder in $GdAl_2$ crystallites [45,46]. The discussed results are consistent with the previously reported ones in $GdAl_2$ nanoparticles [32]. The ZFC curves of the samples milled for 9 and 13 h [the inset of Fig. 6(a)] show an anomaly, i.e., a curve deviation at low temperatures (below 20 K). This feature was not detected in the magnetization curves of the other samples.

Figure 6(b) depicts normalized magnetization (M/H) curves at different magnetic fields for the 13 h sample. The bifurcation between ZFC and FC curves decrease as the field increases as

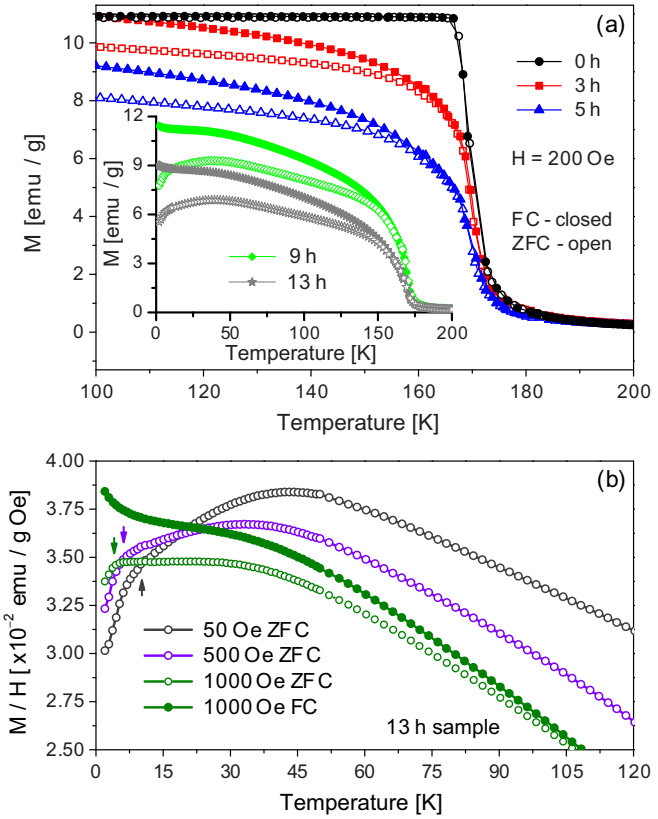

FIG. 6. (a) The temperature dependence of the zero-field-cooling (ZFC) and of the field-cooling (FC) magnetizations for unmilled (0 h) and $GdAl_2$ milled (3 and 5 h) samples under an external magnetic field of $H = 200$ Oe. The inset depicts in detail the ZFC and FC magnetization curves of the samples milled for 9 and 13 h. (b) Magnetization normalized by magnetic field as a function of temperature for different applied magnetic fields for the 13 h sample.

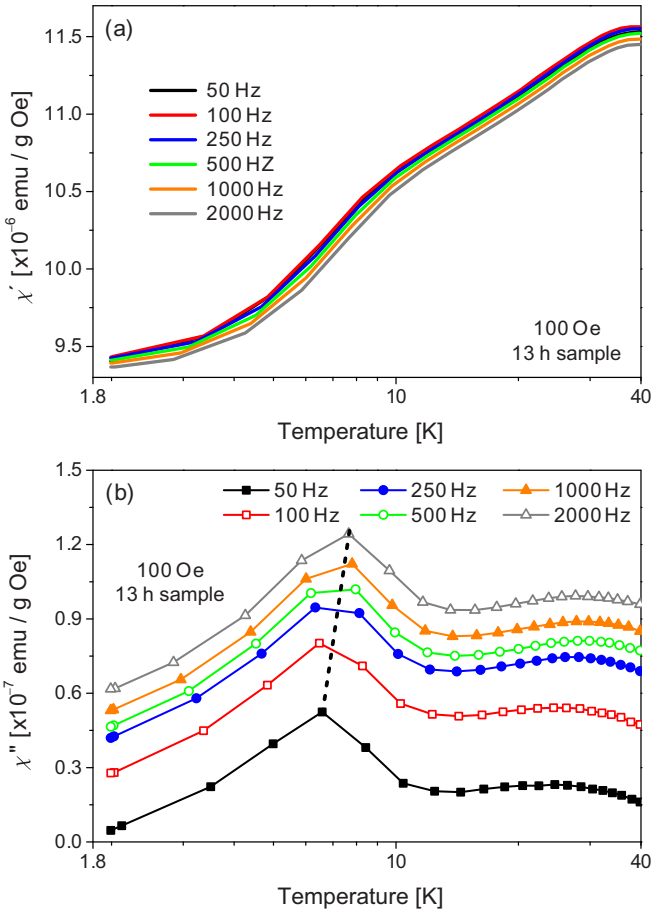

FIG. 7. Temperature dependence of real (a) and imaginary (b) parts of ac susceptibility (100 Oe applied magnetic field) for a frequency variation from 50 to 2000 Hz.

well as the anomaly shifts to lower temperatures as the field increases. Such peculiarities have been observed in systems that exhibit superparamagnetism (SPM), SG, or in cluster-glass (CG) systems [47–49].

To clarify this aspect, ac magnetic susceptibility measurements (consisting of real χ' and imaginary χ'' parts) for a 100 Oe applied magnetic field as a function of the temperature in the frequency range between 0.05 and 2 kHz were conducted. Figure 7 shows in particular the ac magnetic susceptibility for the sample milled for 13 h. The $\chi'(T)$ curve exhibits a broad maximum in the temperature T_f around 10 K. On the other hand, $\chi''(T)$ presents a sharp peak below 10 K whose maximum slightly shifts to higher temperatures with the increase in frequency. In principle, it is possible to distinguish the aforementioned effects by using a frequency-sensitive factor called the Mydosh parameter, considering that the SPM, SG, and CG states have frequency dependences on ac susceptibility. The frequency sensitive factor is given by [50]

$$\Phi = \frac{\Delta T_f}{T_f\left[\Delta\ \log_{10}(\omega)\right]}, \tag{1}$$

where T_f is the temperature of the peak corresponding to the frequency $\omega = 2\pi f$ and ΔT_f is the T_f shift corresponding to a given frequency change. Indeed, the frequency shift on ac susceptibility is different for SPM, SG, and CG systems. Typical values of the Mydosh parameter in the ranges of 0.005–0.01 and 0.03–0.06 are expected for SG and CG, respectively whereas values greater than 0.1 are expected for the SPM system [50]. Using the T_f shift values from the χ'' peak was found to be $\Phi \approx 0.104$ for the 13 h sample. This value lies in the range expected for SPM.

Magnetic hysteresis loops measured for the $GdAl_2$ bulk sample and for the milled samples after the ZFC process at 2 K are shown in Fig. 8(a) and present typical ferromagnetic behaviors. For the bulk sample, the magnetization at $H = 50$ kOe ($M_{50\,\mathrm{kOe}}$) reaches 6.9 μ_B per unit formula. This indicates that the magnetization has not saturated yet (7.94 μ_B for the Gd^{3+} free ion). $M_{50\,\mathrm{kOe}}$ as a function of milling time [Fig. 8(b)] exhibits a gradual decrease as the milling time increases. Indeed, HRTEM images have revealed an amorphous matrix (with embedded nanocrystallites) produced by mechanical milling, i.e., higher milling time increases the amorphous region, decreasing $M_{50\,\mathrm{kOe}}$.

In addition, a very small hysteresis is observed for the bulk sample and for the milled samples. The coercive force H_C as a function of the milling time is displayed in Fig. 8(c). The crystallite size reduction induces an increase in H_C, but the values found are well lower than the expected values for small particles (on the order of kilo-oersteds) [51]. The small

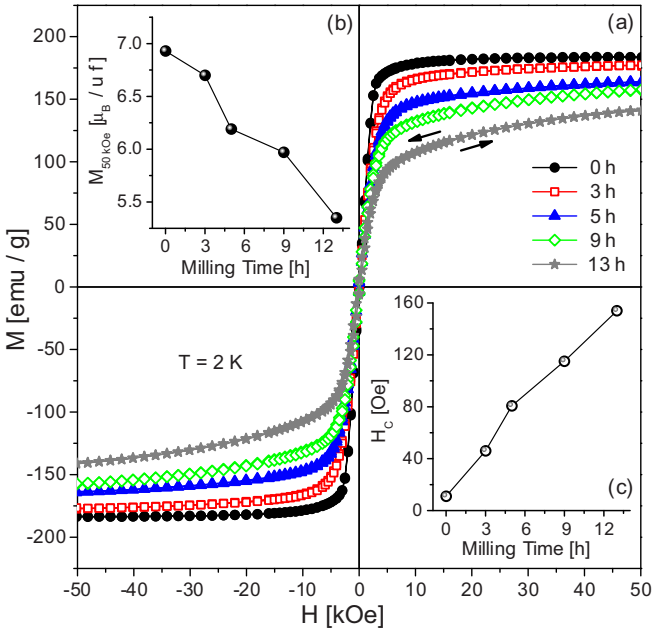

FIG. 8. (a) Magnetic hysteresis loops at 2 K for the samples: $GdAl_2$ bulk (0 h) and for the powders milled for different times: 3, 5, 9, and 13 h. The inset (b) shows $M_{50\,kOe}$ as a function of milling time, whereas the inset (c) shows the coercive force as a function of milling time.

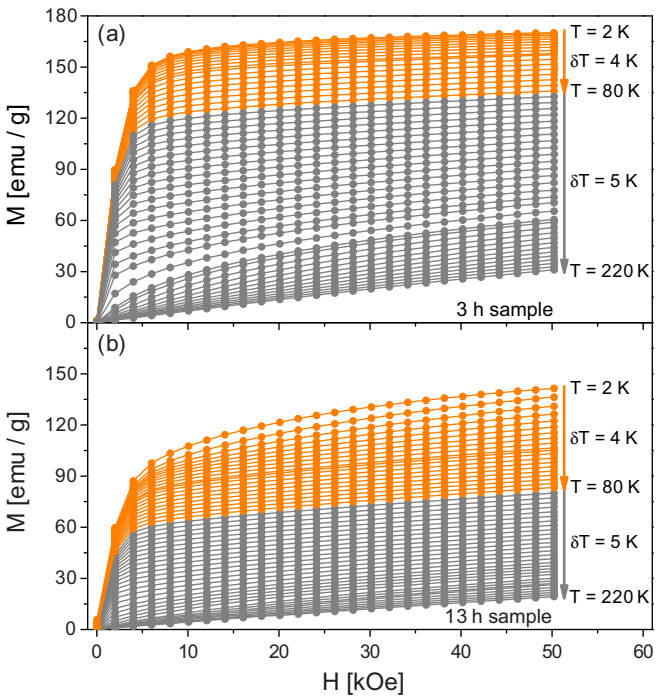

FIG. 9. Isothermal magnetization (depicted in two colors only for a better visualization of the δT interval) as a function of the applied magnetic field for different temperatures measured for the samples milled for (a) 3 h and (b) 13 h.

coercivities obtained for the milled samples are of crucial importance for the practical application of the material in the magnetic refrigeration technology; hysteretic losses are not desired in a thermomagnetic cycle.

Magnetic isothermals $M(H,T)$ as a function of the magnetic field (0–50 kOe) for different temperatures (2–220 K) for the samples milled for 3 and 13 h are presented in Figs. 9(a) and 9(b), respectively. The magnetization increases monotonically with the decrease in T as expected for a ferromagnetic material. The variation of isotherms below 80 K is far more pronounced for the sample milled for 13 h compared to the sample milled for 3 h.

The magnetocaloric effect in terms of a magnetic entropy change ($-\Delta S_M$) was calculated from the isothermal curves by numerical integration of Maxwell's relation [52],

$$\Delta S_M(T,\Delta H) = \int_{H_i}^{H_f} (\partial M/\partial T)_H dH. \quad (2)$$

The temperature dependence of $-\Delta S_M$ calculated for a magnetic-field change of 50 kOe for all $GdAl_2$ samples (bulk and milled) is shown in Fig. 10(a). The maximum value (peak) of entropy change ($-\Delta S_{max}$) around T_C (~170 K) decreases with the crystallite size reduction (milling time increase), and as a result, the peak broadens leading to a tablelike behavior in a large temperature range. The largest tablelike MCE was found for the sample milled for 13 h which corresponds to a (30–165 K) temperature range; comparable to those ones with similar field changes obtained for $Eu_8Ga_{16}Ge_3$-EuO [53], Eu_4PdMg [54], $U_{1-y}R_yGa_2$ [55], $GdCo_xAl_{2-x}$ composites [38], and Gd-Co-Al alloys [56]. Here, the structural disorders induced by the mechanical milling process, which are responsible for a T_C distribution, also support the observed tablelike behavior.

The relative cooling power (RCP) is considered as an important parameter to quantify the heat transferred between the hot and the cold sinks in an ideal refrigeration cycle. The RCP was estimated by using the following approach [57]:

$$RCP = |\Delta S_{max}|\delta_{FWHM}, \quad (3)$$

where δ_{FWHM} stands for the full width at half maximum at the $|\Delta S_M|$ curves. For the first milling times (3 and 5 h), although there are decreases in the $-\Delta S_{max}$ values, the extensive broadenings of the peaks cause increases in the RCP values. For example, the RCP increased from ≈882 J kg^{-1} (unmilled sample) to ≈1000 J kg^{-1} and to ≈906 J kg^{-1} for the samples milled for 3 and 5 h, respectively.

In a close inspection of Fig. 10(a), in particular for the curves of the samples milled for 9 and 13 h, one noticed that when the temperature is lower than 30 K the magnetic entropy change reaches higher values. For the 13 h sample the magnetic entropy change value reaches ≈ 9 J kg^{-1} K^{-1} around 4 K. Surprisingly, this value is on the order of $-\Delta S_{max}$ around T_C (~170 K) obtained for the bulk sample. Thereby, for the 13 h sample we proceed to investigate the temperature dependence of $-\Delta S_M$ for different magnetic-field changes. The results are depicted in Fig. 10(b). As expected, the magnetic entropy change values decrease as ΔH decreases, however, more significantly below 15 K. The increase in $-\Delta S_M$ curves at low temperatures has been predicted for small particle systems that exhibit superparamagnetism [58]. The magnetization variation of a superparamagnetic nanoparticle can be described by the Zeeman energy, thermal-excitation energy, anisotropy-energy barrier, and interaction energy [51]. Such energies provoke an excitation effect but also can act

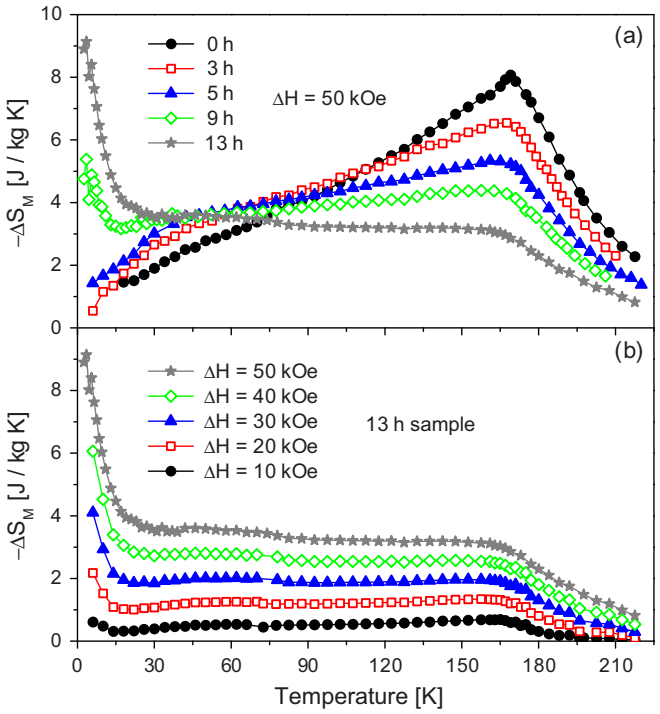

FIG. 10. (a) Temperature dependence of magnetic entropy change ($-\Delta S_M$) calculated for $\Delta H = 50$ kOe for the samples: bulk (0 h) and milled for 3, 5, 9, and 13 h. (b) $-\Delta S_M$ curves for the 13 h sample as a function of the temperature for different magnetic-field changes.

as an obstacle for the rotation of the magnetic moments. Under constant magnetic fields and low temperatures, these four kinds of energies maintain a balance, and the magnetic moments remain blocked. Unbalance caused by subtle changes in these conditions will give rise to alterations in the magnetic moment orientations leading to a large $(\partial M/\partial T)H$ contributing to the magnetic entropy change. Therefore, the MCE increase at lower temperatures is interpreted here as the response of the superparamagnetic nanocrystallites to the magnetic-field change. Furthermore, the magnetocaloric results complement and corroborate the magnetization data inferring to the peak observed in the M_{ZFC} and ac susceptibility curves (13 h sample) a blocking nature. Thereby, magnetocaloric results can also be used as a tool to point out a superparamagnetic state.

It is important to emphasize that usually the superparamagnetic behavior in this type of system has been associated with very small particles (single domain particles with a given critical size in the nanometric range). In the present study, x-ray results for the 9 and 13 h samples show that the average crystallite size is strongly reduced when compared to the bulk sample (from 90 to 24 and 19 nm, respectively). Since the average particle size (micrometric scale) is only slightly diminished with the milling time, the origin of superparamagnetism in these samples, is, therefore, primarily assigned to crystallite size. In principle, the investigated system is a nonideal ensemble of small particles where each particle consists of a nanocrystallite size distribution. Thus, for each particle there is a distribution of intrinsic blocking temperatures T_B coming from nanocrystallites with dimensions below a given critical size. When submitted to temperatures lower than T_B, this fraction of nanocrystallites reaches their blocked states and effectively contributes to the increase in the magnetocaloric effect. Hence, the increase in $-\Delta S_M$ below 15 K observed for the sample milled for 9 h [Fig. 10(a)] indicates that a smaller fraction of nanocrystallites (when compared to the 13 h sample) has reached the critical size for the superparamagnetism. On the other hand, the prominent tablelike magnetocaloric effect in the 13 and 9 h samples is due to a ferromagnetic ordering associated with the larger nanocrystallites.

Finally, the results discussed here can address a better understanding of the spin-glass behavior achieved in mechanically milled $GdAl_2$ samples for very long times: 400 and 1000 h [30,32]. Both studies were essentially based on x-ray diffraction measurements and magnetization data. In the present paper, HRTEM observations, crucial for elucidating the magnetic-structural correlation, reveal that as milling time increases the amorphous region of the particles gradually increases. In this way, with the increase in the amorphous fraction of the particle induced by the milling process (for longer milling times than 13 h) the appearance of cluster glass in $GdAl_2$ particles is expected. Furthermore, for very long milling times as long as 400 or 1000 h, the amorphous fraction becomes the predominant feature as a consequence of mechanical impact. In this case, contributions from the particle-disordered portion overcome the size effect from few nanocrystallites structurally ordered, leading to a spin-glass state, i.e., the macroscopic observation of the magnetization.

IV. CONCLUSIONS

Correlations among structural, magnetic, and magnetocaloric properties in a mechanically milled $GdAl_2$ material were investigated. It was observed that magnetic properties are strongly size dependent. The morphological and structural characterizations by using SEM have shown the occurrence of irregular-shaped micrometric particles after the milling process that has been extended up to 13 h. The average particle size, determined by histograms of SEM images, indicated a decrease of $\approx$7% between 3 and 13 h of the milling time. HRTEM observations have revealed that the microparticles are formed by an amorphous matrix with embedded randomly oriented nanocrystallites. On the particle surface regions, it was possible to identify an amorphous shell, and that, although the thickness is not homogeneous, the average thickness of the shell increases with the milling time. In contrast, x-ray analysis has shown that the average crystallite size was considerably reduced—approximately 43%. Therefore, the decrease in crystallite size has been considered the main effect of the mechanical milling in the used time range. Longer milling times increase the amorphous fraction within the particles and consequently, promote the reduction of the average crystallite size. Structural disorders associated with the crystallite size reduction singularly affect the magnetic properties. Longer milling times cause: (i) a broadening of the ferromagnetic transition that leads to a large (30–165 K) tablelike MCE and (ii) an enhancement in the magnetocaloric effect at lower temperatures (below 30 K) associated with the superparamagnetic behavior originated

from nanocrystallites with dimensions below a given critical size. Lower milling times promote an improvement in the relative cooling power values; for instance, increased from ≈882 J kg^{-1} (bulk sample) to ≈1000 J kg^{-1} for the sample milled for 3 h. A further interesting result is the lack of a significant magnetic hysteresis for milled samples, evidenced by the small coercivity values. Such features make the milled $GdAl_2$ a promising candidate for magnetic refrigeration.

ACKNOWLEDGMENTS

The authors would like to thank the Brazilian funding agencies Conselho Nacional de Desenvolvimento Científico e Tecnológico, Fundação de Amparo à Pesquisa e Desenvolvimento Científico do Maranhão, and Financiadora de Estudos e Projetos for partial financial support.

[1] A. M. Tishin, in *Handbook of Magnetic Materials*, edited by K. H. Buschow (Elsevier, New York, 1999), Vol. 12, p. 395.
[2] V. K. Pecharsky and K. A. Gschneidner, J. Magn. Magn. Mater. **200**, 44 (1999).
[3] C. Zimm, A. Jastrab, A. Sternberg, V. Pecharsky, K. Gschneidner, M. Osborne, and I. Anderson, Adv. Cryog. Eng. **43**, 1759 (1998).
[4] K. A. Gschneidner, V. K. Pecharsky, A. O. Pecharsky, and C. B. Zimm, Mater. Sci. Forum. **69**, 315 (1999).
[5] V. Provenzano, A. J. Shapiro, and R. D. Shull, Nature (London) **429**, 853 (2004).
[6] A. M. Tishin and Y. I. Spichkin, in *The Magnetocaloric Effect and Its Application*, 1st ed., edited by J. M. D. Coey, D. R. Tilley, and D. R. Vij, Series in Condensed Matter Physics (Institute of Physics, Bristol, 2003).
[7] L. M. da Silva, A. O. dos Santos, A. A. Coelho, and L. P. Cardoso, Appl. Phys. Lett. **103**, 162413 (2013).
[8] J. Liu, T. Gottschall, K. P. Skokov, J. D. Moore, and O. Gutfleisch, Nature Mater. **11**, 620 (2012).
[9] R. D. dos Reis, L. M. da Silva, A. O. dos Santos, A. M. N. Medina, L. P. Cardoso, and F. C. G. Gandra, J. Phys.: Condens. Matter **22**, 486002 (2010).
[10] B. G. Shen, J. R. Sun, F. X. Hu, H. W. Zhang, and Z. H. Cheng, Adv. Mater. **21**, 4545 (2009).
[11] A. de Campos, D. L. Rocco, A. M. Carvalho, L. Caron, A. A. Coelho, S. Gama, L. M. da Silva, F. C. G. Gandra, A. O. dos Santos, L. P. Cardoso, P. J. von Ranke, and N. A. de Oliveira, Nature Mater. **5**, 802 (2006).
[12] E. Bruck, J. Phys. D: Appl. Phys. **38**, R381 (2005).
[13] L. Morellon, Z. Arnold, C. Magen, C. Ritter, O. Prokhnenko, Y. Skorokhod, P. A. Algarabel, M. R. Ibarra, and J. Kamarad, Phys. Rev. Lett. **93**, 137201 (2004).
[14] X. Zhou, W. Li, H. P. Linkei, and G. Williams, J. Phys.: Condens. Matter **16**, L39 (2004).
[15] O. Tegus, E. Bruck, H. J. Buschow, and F. R. de Boer, Nature (London) **415**, 150 (2002).
[16] N. A. de Oliveira, P. J. von Ranke, M. V. Tovar Costa, and A. Troper, Phys. Rev. B **66**, 094402 (2002).
[17] V. K. Pecharsky and K. A. Gschneidner, Phys. Rev. Lett. **78**, 4494 (1997).
[18] W. Miller, D. D. Belyea, and B. J. Kirby, J. Vac. Sci. Technol. A **32**, 040802 (2014).
[19] P. Poddara, J. Gassa, D. J. Rebara, S. Srinatha, H. Srikanthac S. A. Morrison, and E. E. Carpenterb, J. Magn. Magn. Mater. **307**, 227 (2006).
[20] X. G. Liu, S. W. Or, B. Li, Z. Q. Ou, L. Zhang, Q. Zhang, D. Y. Geng, F. Yang, D. Li, E. Bruck and Z. D. Zhang, J. Nanopart. Res. **13**, 1163 (2011).
[21] F. Calvo, *Nanoalloys: From Fundamentals to Emergent Applications* (Elsevier, Amsterdam, 2013).
[22] R. Singh, J. Magn. Magn. Mater. **346**, 58 (2013).
[23] E. Roduner, Chem. Soc. Rev. **35**, 583 (2006).
[24] J. R. Health, Science **270**, 1315 (1995).
[25] C. B. Murray, C. R. Kagan, and M. G. Bawendi, Science **270**, 1335 (1995).
[26] X. G. Liu, D. Y. Geng, J. J. Jiang, B. Li, S. Ma, D. Li, W. Liu, and Z. D. Zhang, J. Nanopart. Res. **12**, 1167 (2010).
[27] S. Ma, W. B. Cui, D. Li, N.K. Sun, D. Y. Geng, X. Jiang, and Z. D. Zhang, Appl. Phys. Lett. **92**, 173113 (2008).
[28] X. G. Liu, B. Li, D. Y. Geng, C. X. Shi, F. Yang, D. J. Kang and Z. D. Zhang, J. Phys. D: Appl. Phys. **42**, 045008 (2009).
[29] X. G. Liu, D. Y. Geng, J. Du, S. Ma, B. Li, P. J. Shang, and Z. D. Zhang, Scr. Mater. **59**, 340 (2008).
[30] G. F. Zhou and H. Bakker, Phys. Rev. Lett. **73**, 344 (1994).
[31] G. F. Zhou and H. Bakker, Phys. Rev. B **52**, 9437 (1995).
[32] D. S. Williams, P. M. Shand, T. M. Pekarek, R. Skomski, V. Petkov, and D. L. Leslie-Pelecky, Phys. Rev. B **68**, 214404 (2003).
[33] I. Turek, J. Rusz, and M. Divis, J. Alloys Compd. **431**, 37 (2007).
[34] M. Rotter Lindbaum in *Handbook of Magnetic Materials*, edited by K. H. J. Buschow (Elsevier, New York, 2002), Vol. 14, p. 307.
[35] E. M. Levin, V. K. Pecharsky, and K. A. Gschneidner, J. Appl. Phys. **90**, 6255 (2001).
[36] A. P. Malozemoff and J. P. Jamet, Phys. Rev. Lett. **39**, 1293 (1977).
[37] T. Mizoguchi, T. R. McGuire, S. Kirkpatrick, and R. J. Gambino, Phys. Rev. Lett. **38**, 89 (1977).
[38] H. Fu, R. L. Hadimani, Z. Ma, M. X. Wang, B. H. Teng, and D. C. Jiles, J. Appl. Phys. **115**, 17A914 (2014).
[39] P. O. Ribeiro, B. P. Alho, T. S. T. Alvarenga, E. P. Nóbrega, A. Magnus G. Carvalho, V. S. R. de Souza, A. Caldas, N. A. de Oliveira, and P. J. von Ranke, J. Alloys Compd. **563**, 242 (2013).
[40] D. Jianqiu, Z. Jinming, Y. Jialin, Z. Yinghong, and W. Richu, J. Rare Earths **25**, 783 (2007).
[41] S. Ma, W. F. Li, D. Li, D. K. Xiong, N. K. Sun, D. Y. Geng, W. Liu, and Z. D. Zhang, Phys. Rev. B **76**, 144404 (2007).
[42] A. C. Larson and R. B. Von Dreele, General Structure Analysis System (GSAS), Los Alamos National Laboratory Report No. LAUR 86-748, 2004 (unpublished).
[43] A. I. Gusev and A. A. Rempel, *Nanocrystalline Materials* (CambridgeUniversity Press, Cambridge, U.K., 2003).
[44] S. A. Nepijko and R. Wiesendang, Europhys. Lett. **31**, 567 (1995).
[45] Y. Imry and M. Wortis, Phys. Rev. B **19**, 3580 (1979).
[46] A. J. Millis, Solid State Commun. **126**, 3 (2003).
[47] V. Kumar, R. Kumar, K. Singh, S. K. Arora I. V. Shvets, and R. Kumar, J. Appl. Phys. **116**, 073903 (2014).

[48] B. Venkateswarlu, P. D. Babu, and N. H. Kumar, IEEE Trans. Magn. **50**, 1002004 (2014).
[49] T. Paramanik, T. Samanta, R. Ranganathana, and I. Das, RSC Adv. **5**, 47860 (2015).
[50] J. A. Mydosh, *SPIN GLASSES: An Experimental Introduction* (Taylor & Francis, London, 1993).
[51] B. D. Cullity and C. D. Graham, *Introduction to Magnetic Materials* (Wiley, Hoboken, NJ, 2009).
[52] V. K. Pecharsky and K. A. Gschneidner. J. Appl. Phys. **86**, 565 (1999).
[53] A. Chaturvedi, S. Stefanoski, M.-H. Phan, G. S. Nolas, and H. Srikanth, Appl. Phys. Lett. **99**, 162513 (2011).
[54] L. Li, O. Niehaus, M. Kersting, and R. Pottgen, Appl. Phys. Lett. **104**, 092416 (2014).
[55] L. M. da Silva, A. O. dos Santos, F. C. G. Gandra, L. P. Cardoso, and S. Gama, J. Appl. Phys. **103**, 07B308 (2008).
[56] H. Fu, Z. Ma, X. J. Zhang, D. H. Wang, B. H. Teng, and E. A. Balfour, Appl. Phys. Lett. **104**, 072401 (2014).
[57] Q. Zhang, X. G. Liu, F. Yang, X. G. Zhao, D. J. Kang, and Z. D. Zhang, J. Phys. D: Appl. Phys. **42**, 055011 (2009).
[58] R. D. McMichael, R. D. Shull, L. J. Swartzendruber, L. H. Bennett, and R. E. Watson, J. Magn. Magn. Mater. **111**, 29 (2013).